ACS Photonics

Article

pubs.acs.org/journal/apchd5

Infrared Perfect Absorbers Fabricated by Colloidal Mask Etching of Al–Al_2O_3–Al Trilayers

Thang Duy Dao,*[,†,‡,§] Kai Chen,[†,‡] Satoshi Ishii,[†,‡] Akihiko Ohi,[†] Toshihide Nabatame,[†,‡] Masahiro Kitajima,[†,‡,⊥] and Tadaaki Nagao*[,†,‡]

[†]International Center for Materials Nanoarchitectonics, National Institute for Materials Science (NIMS), 1-1 Namiki, Tsukuba, Ibaraki 305-0044, Japan

[‡]CREST, Japan Science and Technology Agency, 4-1-8 Honcho, Kawaguchi, Saitama 332-0012, Japan

[⊥]LxRay Co., Ltd., 3-28-22, Koshienguchi, Nishinomiya, Hyogo, 663-8113, Japan

[§]Graduate School of Materials Science, Nara Institute of Science and Technology, 8916-5 Takayama, Ikoma, Nara 630-0192, Japan

Supporting Information

ABSTRACT: We propose a combined fabrication method of reactive ion etching and large-scale colloidal mask to fabricate mid-infrared metamaterial perfect absorbers using aluminum–aluminum oxide-aluminum trilayers. The absorptivities of the fabricated samples reached as high as 98% and the absorption bandwidths were comparable to those of the absorbers based on gold or silver. Following Kirchhoff's law, their emission spectra exhibited sharp single emission peaks indicating high potential as narrow-band infrared emitters. The results obtained here demonstrate that earth-abundant aluminum is a high-performance plasmonic materials in the mid-infrared range, and open up a route for fabricating cost-effective scalable plasmonic devices such as efficient light harvesting structures, thermal emitters, and infrared sensors.

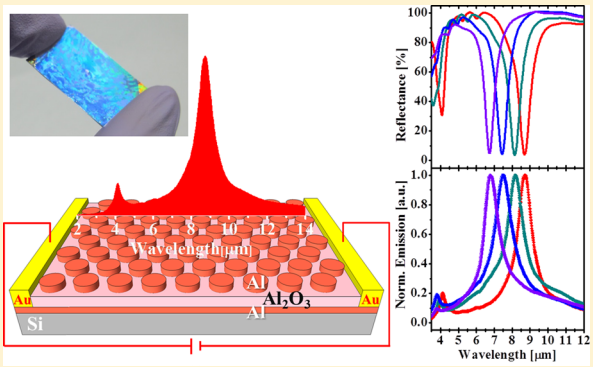

KEYWORDS: *aluminum, plasmonic metamaterial, perfect absorber, thermal emission, colloidal lithography*

Radiative heat transfer and thermal absorption have become of serious importance in modern microelectronics technology. Ranging from heat sinks and radiators in computers, infrared gas sensing to thermophotovoltaics, there are a number of demands for improving the thermal absorptivity and emissivity. Among many efficient heat absorbers, artificial subwavelength structures made of metals, known as plasmonic metamaterials, have gained much attention because they allow light harvesting and manipulation in deep subwavelength scale. With appropriate metamaterial designs they can exhibit nearly 100% narrow- or broad-band absorption at desired wavelength with wide tunability,[1−9] which are so-called perfect absorbers (PAs). Perfect absorbers have found a wide range of applications in photonics and optoelectronics such as light emitting devices,[10−15] plasmonic refractive index sensors,[16] surface-enhanced infrared absorption spectroscopy,[17,18] and CO_2 sensors,[19] to name a few.

According to Kirchhoff's law of thermal radiation, an absorber can emit thermal radiation at the same wavelength of its absorption spectrum when it is heated. Narrow-band selective thermal radiation in the infrared (IR) region is expected to be utilized for various applications such as thermophotovoltaics[20−22] and nondispersive infrared (NDIR) spectroscopy.[23] Various periodic structures using different materials have been demonstrated as narrow-band thermal emitters, which include devices based on photonic crystals,[24−26] plasmonic grating surfaces of tungsten[27] or steel,[28] and hole arrays of Ag–SiO_2–Ag.[29] Among the structures mentioned above, patterned plasmonic metal–insulator–metal (MIM) structures have attracted tremendous attention recently for selective thermal emitters[12−15,19] due to their excellent controllability and the ease of fabrication.

With regard to plasmonic materials, gold (Au) and silver (Ag) are the two most widely used materials in the visible (VIS), IR, and even terahertz (THz) regions. Aluminum (Al) is known to be an excellent plasmonic material whose nanostructures can give plasmon resonances from the deep ultraviolet (DUV) to the VIS region.[30−34] In the IR region, Al shows higher losses than Au and Ag but it still exhibits excellent metallic response indicating its high potential as a typical free-electron metal for IR plasmonic devices.[35,36] Because of its natural abundance, easy handling, and workability, Al can be an excellent candidate for IR plasmonic devices.

In this work, we developed a facile fabrication method using colloidal masks to fabricate large-scale MIM perfect absorbers in the middle IR (MIR) region. The aluminum perfect absorbers (Al-PAs) were simulated by rigorous coupled-wave

Received: April 13, 2015
Published: June 2, 2015

DOI: 10.1021/acsphotonics.5b00195
ACS Photonics 2015, 2, 964–970

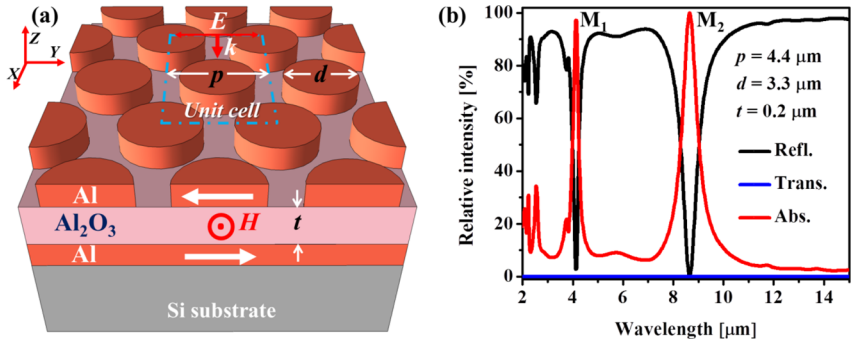

Figure 1. (a) Schematic design of the Al-PA with definitions of geometrical parameters: periodicity p, diameter of Al disk resonator d, and insulator thickness t. The incident electromagnetic fields propagate along the $-z$-axis and the electric field is polarized in x direction. (b) Simulated spectra of an Al-PA with p = 4.4, d = 3.3, and t = 0.2 μm. The absorptivities of the two resonance peaks at 4.16 μm (M_1) and 8.65 μm (M_2) were 97.2 and 99.9%, respectively.

analysis (RCWA) to optimize the geometry parameters. The designed structures were fabricated by choosing the polystyrene (PS) sphere size for the masks and controlling the etching time in the colloidal lithography. The fabricated Al-PAs showed excellent agreement with the RCWA simulations and exhibited near perfect absorption (ca. 98%) with narrow bandwidth (fwhm < 0.75 μm), which are comparable to the structures made of Au or Ag. The resonant wavelengths were readily tuned from 3 to 9 μm by adjusting the geometrical parameters. By moderately heating up the Al-PAs, narrow-band thermal emissions at their corresponding absorption bands were observed. The use of cost-effective Al as a plasmonic material, together with the simple fabrication technique developed in this work, will greatly expand the possibility and applications of plasmonic devices in the IR region, which are not limited to absorbers or emitters.

RESULTS AND DISCUSSION

Proposed Structure. Our proposed Al-MIM structure is shown in Figure 1a: a hexagonal array of Al disk resonators is placed on the top and an Al film separated by an Al_2O_3 insulator is placed at the bottom. The Al film is chosen to have a thickness of 0.1 μm to eliminate transmission of infrared radiation through the structure, and it also serves as a joule heater when current is applied to study thermal emissions from the sample. In the present Al-PA devices, the thickness of Al disk resonator was fixed at 0.1 μm, and the resonant wavelength and absorptivity of the MIM structure are controlled by tuning the periodicity p, the diameter of Al disk d, and the thickness of the insulator t. For example, Figure 1b shows the simulated spectra of an Al-PA structure with its parameters of p = 4.4 μm, d = 3.3 μm, and t = 0.2 μm. The absorptivity at wavelength λ is given by $A(\lambda) = 1 - R(\lambda) - T(\lambda)$, where $R(\lambda)$ and $T(\lambda)$ are the reflectance and transmittance of the structure, respectively. Since the transmission of the Al-PA structure is almost zero, the absorptivity of an Al-PA is simply given by $A(\lambda) = 1 - R(\lambda)$. The proposed structure has two narrow resonance bands, a short-wavelength resonance indicated as M_1 at 4.16 μm with an absorptivity of 97.2%, and a main long-wavelength resonance indicated as M_2 at 8.65 μm with absorptivity up to 99.9%. It should be noted that Al has relatively high losses in the VIS to NIR region, which are the drawbacks in plasmonic applications. On the other hand, it has excellent metallic response in the IR region with larger negative real part of permittivity than Au, Ag, and tungsten (W; Supporting Information, Figure S1a).[37,38] This indicates that, in the IR region, high losses in Al can be compensated by the metallic response and Al can be a material of choice for thermal absorbers and emitters. For comparison, simulations of the absorptivity of Au, Ag, and W were also performed and shown in the Supporting Information, Figure S1b. The results indicate that perfect IR light absorption can be achieved with Al and W, which are known to be less advantageous in the VIS region for plasmonic applications. In spite of the expected advantage of using Al in the IR region, however, applications of Al structures for PAs are rather limited so far.[35,36]

Optical Properties. To elucidate the optical properties of the Al-PA, further simulations were performed as shown in Figure 2. The resonant wavelengths of the Al-PA continuously shift as the diameter of the Al disk (Figure 2a) or the periodicity varies (Figure 2b). As we can see in Figure 2a, with the periodicity p and insulator thickness t fixed at 4.4 and 0.2 μm, respectively, M_2 gradually increases with increasing the diameter of the Al disk, while M_1 is hardly dependent on the

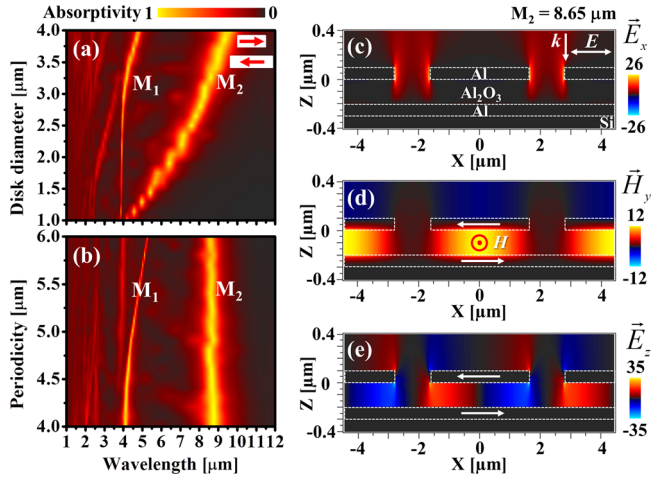

Figure 2. Simulated optical properties of the designed Al-PAs. (a) The dependence of resonance wavelengths on the Al disk diameters in the Al-PAs. The periodicity of the Al-PA was fixed at 4.4 μm. (b) The periodicity-dependent resonant wavelengths of the Al-PAs. The disk diameters of the Al-PAs were fixed at 3.3 μm. (c–e) Electromagnetic field distributions in Al-PA structure under polarized excitation at magnetic resonance at 8.65 μm. The electric fields propagate along $-z$-axis and oscillate in x direction. The amplitudes of the electric and magnetic incident fields were normalized to 1. White arrows in (d) and (e) illustrate the charge motions in top and bottom Al layers.

DOI: 10.1021/acsphotonics.5b00195
ACS Photonics 2015, 2, 964–970

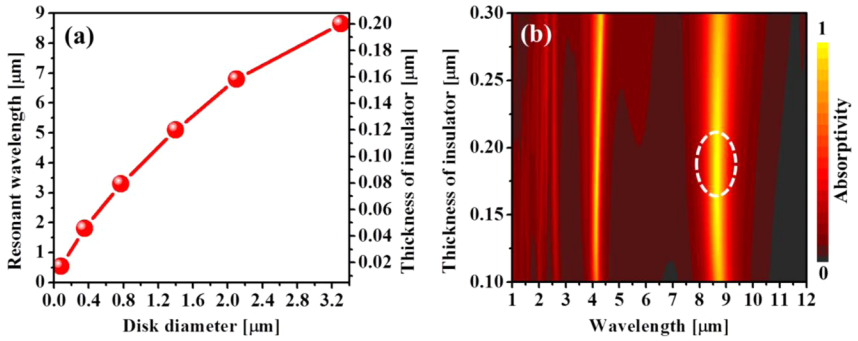

Figure 3. (a) The simulated resonant wavelengths at magnetic mode with perfect absorption ranging from 0.5−9 μm by varying the diameter of Al disk with suitable periodicity, p (or suitable PS spheres with variable diameters ranging from 0.2 to 4.4 μm) and insulator thickness. (b) The simulated dependence of the absorptivity on the insulator thickness (p = 4.4 μm, d = 3.3 μm). The dashed oval shows highest absorption efficiency near 100% corresponding to the insulator thickness of about 0.2 μm.

diameter of Al disk d when d is small compared to the resonant wavelength at M_1. When d is comparable to the resonant wavelength at M_1, M_1 becomes slightly dependent on the Al disk diameter d. In contrast, opposite behavior is observed for the effect of the periodicity. As shown in Figure 2b, M_2 shows little dependence on the periodicity, while M_1 gradually shifts toward longer wavelength when the periodicity increases. In the Al-PA, M_1 is related to surface plasmon (SP), photonic mode coupling (or delocalized plasmon),[5,39] which strongly depends on the periodicity of the structure. On the other hand, M_2 is related to the localized surface plasmon (LSP) resonances, which are strongly dependent on the diameters of the Al disks. At M_2, the dipole oscillation of the free electrons in the top Al disk resonator induces an antiparallel dipole oscillating in the bottom layer, resulting in the formation of an electric current loop to effectively induce a magnetic dipole. Thus, this type of resonance is often referred to as the "magnetic mode".

To further verify the underlying absorption mechanism of these two resonance modes, we performed simulations to visualize the electromagnetic field distributions, as shown in Figure 2c−e at 8.65 μm. The geometrical parameters chosen in the simulation were p = 4.4 μm, d = 3.3 μm, and t = 0.2 μm. The incident electric and magnetic field amplitudes were normalized to 1. The electric field E_x is enhanced up to 26× (Figure 2c) and located at the edges of the Al disks, while the magnetic field induced by the electric loop current resides inside the insulator layer (Figure 2d). The induced electric field E_z clearly indicates that these "magnetic hot-spots" are associated with the looplike nature of the charge motion (Figure 2e). As a comparison, the field distribution of the SP-photonic coupling mode is shown in Figure S2 in the Supporting Information. Note that its absorptivity can be easily reduced by the presence of defects and imperfection in periodicity.

We further simulated the dependence of the resonant wavelengths on the resonator thickness (Supporting Information, Figure S3a) and on the incident light polarization (Supporting Information, Figure S3b). The thickness of the Al disk resonator does not affect M_2 and M_1 modes very much (except slight red-shifts) provided that the thickness is larger than 50 nm. Their resonant wavelengths stay unchanged with polarization changing from 0 to 90°, which is beneficial to working with unpolarized light including sunlight.

As we described above, the resonance wavelength of the M_2 mode is strongly dependent on the diameter of the Al-disk resonator. Here, the detailed analyses of this tunability ranging from 0.5−9 μm are shown in Figure 3a. The thickness of the bottom Al film was fixed at 0.1 μm and the thickness of Al disk resonators were 0.1 μm for IR range and 0.04 μm for VIS range. The absorptivity of the Al-PAs can be optimized by tuning the thickness of the insulator, which is demonstrated for M_2 mode in Figure 3b (p = 4.4 μm, d = 3.3 μm). Thus, by choosing the suitable periodicity (by choosing the PS sphere size), tuning the Al disk diameters and optimizing the insulator thickness, we can tune the resonant wavelength of the magnetic mode in a wide range from VIS to MIR (Figure 3a). For example, a perfect absorption at 6.8 μm can be achieved by choosing the periodicity, Al disk resonator, and insulator thickness to be 3.0, 2.1, and 0.15 μm, respectively.

Fabrication Method. We realized large-scale IR plasmonic Al-PAs by combining colloidal lithography with reactive ion etching (RIE) technique. Colloidal lithography[40,41] is a simple but versatile and inexpensive technique to fabricate large-scale periodic structures without using expensive lithography processes. Colloidal spheres with size ranging from several hundreds of nanometers to several microns are commercially available, facilitating tenability of the structures. Quite recently, Walter et al. have reported the combination of colloidal lithography and RIE technique using selective incorporation of a sacrificial Ni layer to fabricate random Au disks for NIR perfect absorption.[42] Here we employed an etching process twice and we can keep close-packed periodicity. The detailed step-by-step fabrication in the present work is shown in Figure 4. First, an Al−Al_2O_3−Al trilayer was sputtered on a Si

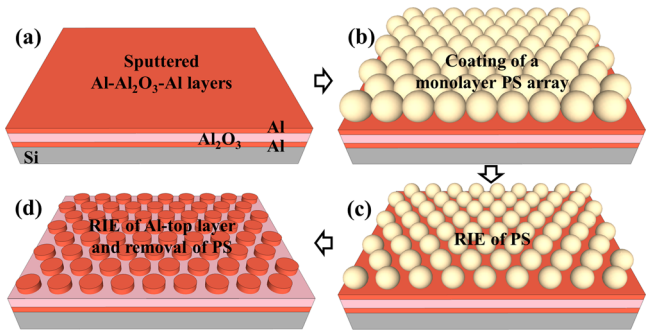

Figure 4. Illustration of the fabrication process. (a) Sputtered Al−Al_2O_3−Al film on a Si(100) substrate. (b) Self-assembled monolayer of PS spheres in close-packed hexagonal array. (c) Shrunk PS mask after the RIE process with oxygen. (d) Final structure of the device after RIE of the Al top layer and removal of the PS mask.

DOI: 10.1021/acsphotonics.5b00195
ACS Photonics 2015, 2, 964−970

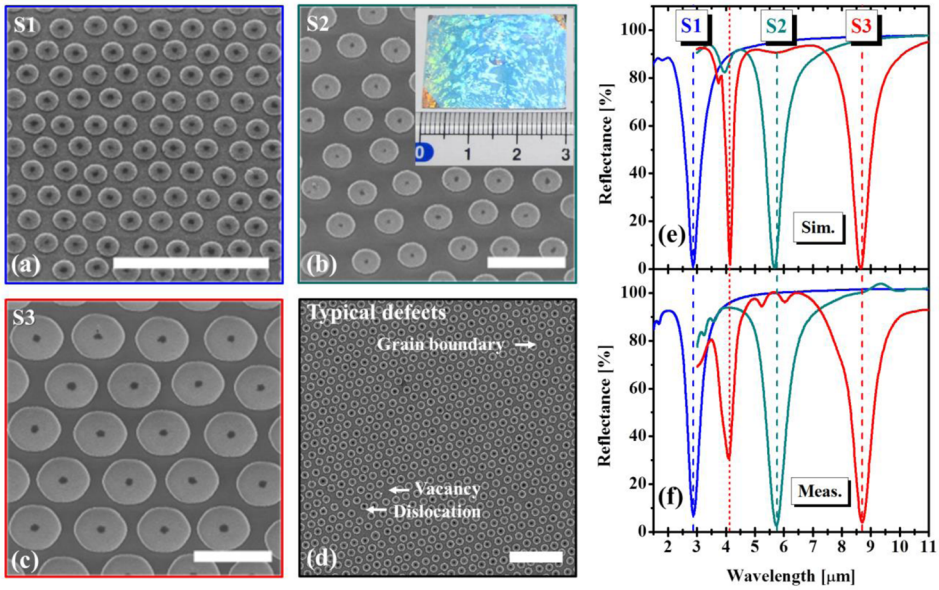

Figure 5. (a–c) 30° titled-view SEM images of three fabricated Al-PAs with their resonances as designed: (a) S1 (p = 1.1 μm, d = 0.7 μm, t = 0.05 μm) at 2.85 μm, (b) S2 (p = 3.0 μm, d = 1.7 μm, t = 0.15 μm) at 5.67 μm, and (c) S3 (p = 4.4 μm, d = 3.3 μm, t = 0.2 μm) at 8.65 μm. (d) Typical defects of the fabricated samples. The inset in (b) is a photograph of a fabricated Al-PA of 2 × 3 cm^2. The scale bar is 5 μm in each image. (e, f) Simulated and measured reflectance spectra of sample S1, S2, and S3 shown in (a–c).

substrate with the optimized thickness as discussed in the previous section (Figure 4a). The layered film was then coated with a monolayer of PS spheres to form a close-packed hexagonal array (Figure 4b). The size of the PS mask was reduced by the RIE process using oxygen gas (Figure 4c). Then, Al disk resonators were formed by milling the PS-masked Al top layer with a mixture of BCl_3 and Cl_2 gases, and finally, the PS mask was removed (Figure 4d). The resonance of the Al-PA can be precisely tuned by changing the size of the PS mask with accurate control of the etching time (Supporting Information, Figure S4).

Fabricated Samples. Following the design principle shown in Figure 3, we fabricated a series of Al-PAs with resonant modes in the IR region. Figure 5a–c shows 30° titled-view SEM images of three fabricated Al-PAs. Figure 5d exemplifies some typical defects incorporated during the deposition of the colloidal masks, including dislocation, vacancy, and grain boundary defects. The inset in Figure 5b shows a photograph of a typical Al-PA sample fabricated on a 2 × 3 cm^2 substrate. The periodicity p, Al disk diameter d, and thickness of Al_2O_3 insulator were optimized to realize narrow-band resonances at 2.85 μm (sample S1: p = 1.1 μm, d = 0.7 μm, t = 0.05 μm), at 5.67 μm (sample S2: p = 3.0 μm, d = 1.7 μm, t = 0.15 μm), and at 8.65 μm (sample S3: p = 4.4 μm, d = 3.3 μm, t = 0.2 μm). Figure 5e,f shows the simulated and measured reflectance spectra of the three fabricated samples. The experimental results were in very good agreement with the simulation results, where the magnetic mode M_2 shows as high absorptivity as 98% with a narrow-band of 0.75 μm (full width at half-maximum). The SP-photonic coupling mode M_1 at 4.16 μm (sample S3) shows near 100% absorptivity in the simulation, but the experimental counterpart shows a lower absorptivity of 68% due to the lattice imperfections, as shown in Figure 5d (SP-photonic coupling modes of samples S1 and S2 are not shown). The fabricated Al-PAs exhibit high absorptivity in a wide-range incident angle as we can see in both simulation and measurement (Supporting Information, Figure S5). The main magnetic mode M_2 shows no incident angle dependence, as this mode assumes a localized cavity-like nature within the disk, while the M_1 mode assumes a polaritonic wave-like nature along the surface and shows strong incident angle dependence.

Selective Thermal Emitters. In this section, we discuss the thermal radiation from the Al-PAs. We designed four Al-PAs whose resonant wavelengths are at 6.73 μm (S3a), 7.46 μm (S3b), 8.15 μm (S3c), and 8.65 μm (S3d). All the samples were fabricated using 4.4 μm PS spheres to have the same periodicity of 4.4 μm. Figure 6a shows the simulated reflectance spectra of the Al-PAs with absorptivity higher than 96%. The Al-PAs were fabricated on 0.5 × 3 cm^2 Si substrates (Supporting Information, Figure S6a–e). Figure 6b shows the measured reflectance spectra of the fabricated devices. The measured spectra show near-100% absorptivity at the magnetic resonance modes M_2, which excellently match to the simulated results. In contrast, the measured spectra of SP-photonic coupling modes M_1 show lower absorptivities compared to simulations, which is due to the lattice imperfection as discussed above. To characterize the thermal radiation of Al-PAs, DC currents were applied to resistively heat the bottom Al layers of the samples, and the emission spectra were collected by an FT-IR spectrometer (see schematic in the Supporting Information, Figure S6f). Figure 6c shows the normalized emission spectra of the Al-PAs moderately heated at 250 °C in ambient air. The wavelengths of the selective thermal emissions were identical to the absorption wavelengths, which clearly follows Kirchhoff's law of thermal radiation. The bandwidths of the emission peaks were slightly broader compared to those reflectance dips, which might be caused by the thermal expansion and phonon excitations of the insulating layer and Al disk resonators. It should be noted that a *quasi-monochromatic* thermal emission is realized at the wavelengths of magnetic M_2 modes as the maximum intensity in the blackbody radiation lies in this wavelength region around 100–300 °C (Supporting Information, Figure S7). Our experimental results demonstrate the

DOI: 10.1021/acsphotonics.5b00195
ACS Photonics 2015, 2, 964–970

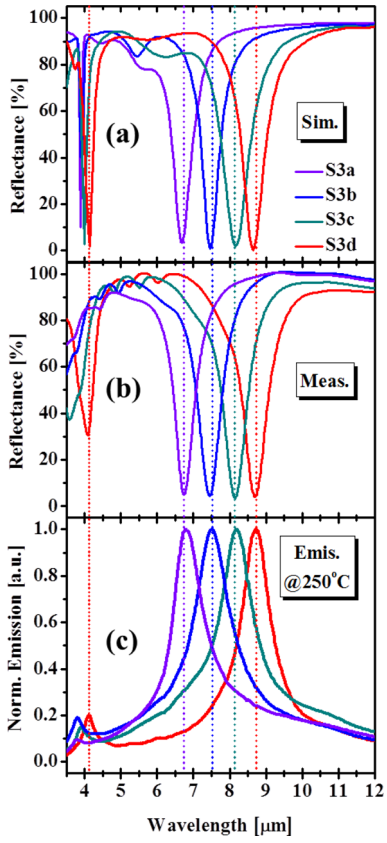

Figure 6. (a) Simulated and (b) measured reflectance spectra of the samples S3a–d. (c) Emission spectra of samples S3a–d heated at 250 °C. The peak positions of the emissions match to the dips in reflectance spectra.

tunability of the narrow-band thermal emission by tuning the diameter of the Al disk resonators.

CONCLUSION

We demonstrated the use of Al for plasmonic perfect absorbers and emitters in the mid-infrared region. For this purpose, we developed a method which combines colloidal lithography and RIE as a flexible and versatile method for fabricating large-scale samples on the order of square centimeters. The simulations showed that the MIM Al-PA with hexagonally arranged Al disks exhibited two narrow-band resonances and high absorptivity. The short-wavelength mode M_1 is attributed to SP-photonic coupling and is strongly dependent on the periodicity. The long-wavelength M_2 mode is magnetic resonance and is strongly dependent on the diameter of the Al disk resonator but is hardly dependent on the periodicity. The fabricated Al-PAs devices showed narrow absorption bands ranging from 3 to 9 μm, with absorptivity up to 98%. As thermal emitters, the Al-PAs exhibited single-peaked quasi-monochromatic emissions. Although we only demonstrated perfect absorptions and selective thermal emissions, the potential applications of Al-PAs in MIR include, but not limited to, wavelength-selective IR photodetectors, surface-enhanced IR absorption spectroscopy, IR surface plasmon resonance (IR-SPR) sensors, thermophotovoltaic, and heat energy harvesting devices.

METHODS

Simulations. The RCWA technique was employed to calculate the spectra of Al-PAs (DiffractMOD, RSoft). The electromagnetic fields distributed around Al-PAs were calculated using the finite-difference time-domain (FDTD) method (FullWAVE, RSoft). The dielectric functions of Al, Au, Ag, W, and Si were taken from the literature,[38] and the dielectric function of Al_2O_3 was taken from literature.[37] The model of Al-PAs device was performed in a cad layout (RSoft CAD), with the unit cell as shown in Figure 1a. For both RCWA and FDTD simulations, the excitation electromagnetic field propagates along the $-z$-axis and the electric field oscillates along the x-axis. The index resolution and grid size in the RCWR and FDTD simulations were set to 10 nm.

Al-PA Sample Fabrication. The Al–Al_2O_3–Al films were deposited on top of Si(100) substrates using DC and RF sputtering methods (i-Miller CFS-4EP-LL, Shibaura). The thicknesses of the films from bottom to top were 0.1, 0.05–0.2 μm (depends on the design), and 0.1 μm, respectively. Polystyrene (Polybead Polystyrene Microspheres - Polysciences) spheres with suitable sizes were used for coating a monolayer on top of sputtered Al–Al_2O_3–Al films. In brief, the Al–Al_2O_3–Al films on Si substrates were placed in a plastic box placed with a 10° tilted angle. The plastic box was then filled up with deionized water. A monolayer of PS spheres was created on the water surface by using a glass slide tilted at 30°. Finally, a monolayer of PS spheres was formed on the layered Al–Al_2O_3–Al films by using a micropump to drain the water in a plastic box. The size of the PS mask was reduced by RIE technique using oxygen gas (20 sccm, APC pressure 1 Pa, antenna RF power 200 W, bias RF power 5 W, Ulvac CE-300I) which gives the etching rate of 3.1 nm/second (Supporting Information, Figure S3). The diameters of Al disk resonators were well-controlled by controlling the size of PS masks. The Al disk resonators were obtained by etching the top Al layer masked by the PS layer at an etching rate of 0.82 nm/second (dual-gases BCl_3/Cl_2, 3/3 sccm, APC pressure 0.15 Pa, antenna RF power 50 W, bias RF power 10 W, Ulvac CE-300I). The MIM Al-PAs were finally formed by removing the PS masks and carefully cleaning with toluene and methanol. In the thermal emitter application, a 0.1 μm thick Au film was thermally deposited at the two ends of the samples as two contacts.

IR Spectroscopy of Al-PAs. The reflectance spectra of the Al-PAs were taken using a Fourier transform infrared (FTIR) spectrometer (Nicolet iS50R FT-IR Thermo Scientific) with a liquid-nitrogen-cooled mercury cadmium telluride (MCT) detector and a KBr beam splitter. A 0.1 μm Au film deposited on Si substrate was used as the reference. To measure the emission spectra, the Al-PAs fabricated on 0.5 × 3 cm^2 Si (100) substrates (Supporting Information, Figure S6) were heated by applying a sufficient DC current in the Al film through Au contacts. The temperatures of the Al-PAs emitters were measured using a thermocouple and controlled by changing the applied current. Then the thermal radiation from Al-PA emitters were collected by the FTIR spectrometer equipped with two concave Al mirrors.

ASSOCIATED CONTENT

Supporting Information

Contains simulated optical properties, fabrication procedure, and measured optical spectra of the Al-PAs. The Supporting Information is available free of charge on the ACS Publications website at DOI: 10.1021/acsphotonics.5b00195.

DOI: 10.1021/acsphotonics.5b00195
ACS Photonics 2015, 2, 964–970

AUTHOR INFORMATION

Corresponding Authors

*E-mail: dao.duythang@nims.go.jp.
*E-mail: nagao.tadaaki@nims.go.jp.

Notes

The authors declare no competing financial interest.

ACKNOWLEDGMENTS

The authors would like to thank Mr. Hidefumi Iga and Mr. Katsumi Ohno in MANA Foundry at NIMS for their advice in RIE and sputtering processes.

REFERENCES

(1) Landy, N.; Sajuyigbe, S.; Mock, J.; Smith, D.; Padilla, W. Perfect Metamaterial Absorber. *Phys. Rev. Lett.* **2008**, *100*, 207402.
(2) Avitzour, Y.; Urzhumov, Y.; Shvets, G. Wide-Angle Infrared Absorber Based on a Negative-Index Plasmonic Metamaterial. *Phys. Rev. B* **2009**, *79*, 045131.
(3) Hao, J.; Wang, J.; Liu, X.; Padilla, W. J.; Zhou, L.; Qiu, M. High Performance Optical Absorber Based on a Plasmonic Metamaterial. *Appl. Phys. Lett.* **2010**, *96*, 251104.
(4) Wu, C.; Neuner, B.; Shvets, G.; John, J.; Milder, A.; Zollars, B.; Savoy, S. Large-Area Wide-Angle Spectrally Selective Plasmonic Absorber. *Phys. Rev. B* **2011**, *84*, 075102.
(5) Pu, M.; Hu, C.; Wang, M.; Huang, C.; Zhao, Z.; Wang, C.; Feng, Q.; Luo, X. Design Principles for Infrared Wide-Angle Perfect Absorber Based on Plasmonic Structure. *Opt. Express* **2011**, *19*, 17413−17420.
(6) Fang, Z.; Zhen, Y.-R.; Fan, L.; Zhu, X.; Nordlander, P. Tunable Wide-Angle Plasmonic Perfect Absorber at Visible Frequencies. *Phys. Rev. B* **2012**, *85*, 245401.
(7) Feng, R.; Ding, W.; Liu, L.; Chen, L.; Qiu, J.; Chen, G. Dual-Band Infrared Perfect Absorber Based on Asymmetric T-Shaped Plasmonic Array. *Opt. Express* **2014**, *22*, A335−A343.
(8) Aydin, K.; Ferry, V. E.; Briggs, R. M.; Atwater, H. A. Broadband Polarization-Independent Resonant Light Absorption Using Ultrathin Plasmonic Super Absorbers. *Nat. Commun.* **2011**, *2*, 517.
(9) Feng, Q.; Pu, M.; Hu, C.; Luo, X. Engineering the Dispersion of Metamaterial Surface for Broadband Infrared Absorption. *Opt. Lett.* **2012**, *37*, 2133−2135.
(10) Ikeda, K.; Miyazaki, H. T.; Kasaya, T.; Yamamoto, K.; Inoue, Y.; Fujimura, K.; Kanakugi, T.; Okada, M.; Hatade, K.; Kitagawa, S. Controlled Thermal Emission of Polarized Infrared Waves from Arrayed Plasmon Nanocavities. *Appl. Phys. Lett.* **2008**, *92*, 021117.
(11) Miyazaki, H. T.; Ikeda, K.; Kasaya, T.; Yamamoto, K.; Inoue, Y.; Fujimura, K.; Kanakugi, T.; Okada, M.; Hatade, K.; Kitagawa, S. Thermal Emission of Two-Color Polarized Infrared Waves from Integrated Plasmon Cavities. *Appl. Phys. Lett.* **2008**, *92*, 141114.
(12) Ye, Y.-H.; Jiang, Y.-W.; Tsai, M.-W.; Chang, Y.-T.; Chen, C.-Y.; Tzuang, D.-C.; Wu, Y.-T.; Lee, S.-C. Localized Surface Plasmon Polaritons in Ag/SiO_2/Ag Plasmonic Thermal Emitter. *Appl. Phys. Lett.* **2008**, *93*, 033113.
(13) Diem, M.; Koschny, T.; Soukoulis, C. Wide-Angle Perfect Absorber/Thermal Emitter in the Terahertz Regime. *Phys. Rev. B* **2009**, *79*, 033101.
(14) Liu, X.; Tyler, T.; Starr, T.; Starr, A. F.; Jokerst, N. M.; Padilla, W. J. Taming the Blackbody with Infrared Metamaterials as Selective Thermal Emitters. *Phys. Rev. Lett.* **2011**, *107*, 045901.
(15) Chen, H.-H.; Hsiao, H.-H.; Chang, H.-C.; Huang, W.-L.; Lee, S.-C. Double Wavelength Infrared Emission by Localized Surface Plasmonic Thermal Emitter. *Appl. Phys. Lett.* **2014**, *104*, 083114.
(16) Liu, N.; Mesch, M.; Weiss, T.; Hentschel, M.; Giessen, H. Infrared Perfect Absorber and Its Application As Plasmonic Sensor. *Nano Lett.* **2010**, *10*, 2342−2348.
(17) Chen, K.; Adato, R.; Altug, H. Dual-Band Perfect Absorber for Multispectral Plasmon-Enhanced Infrared Spectroscopy. *ACS Nano* **2012**, *6*, 7998−8006.
(18) Li, Y.; Su, L.; Shou, C.; Yu, C.; Deng, J.; Fang, Y. Surface-Enhanced Molecular Spectroscopy (SEMS) Based on Perfect-Absorber Metamaterials in the Mid-Infrared. *Sci. Rep.* **2013**, *3*, 2865.
(19) Miyazaki, H. T.; Kasaya, T.; Iwanaga, M.; Choi, B.; Sugimoto, Y.; Sakoda, K. Dual-Band Infrared Metasurface Thermal Emitter for CO_2 Sensing. *Appl. Phys. Lett.* **2014**, *105*, 121107.
(20) Snyder, G. J.; Toberer, E. S. Complex Thermoelectric Materials. *Nat. Mater.* **2008**, *7*, 105−114.
(21) Wang, L. P.; Zhang, Z. M. Wavelength-Selective and Diffuse Emitter Enhanced by Magnetic Polaritons for Thermophotovoltaics. *Appl. Phys. Lett.* **2012**, *100*, 063902.
(22) Lenert, A.; Bierman, D. M.; Nam, Y.; Chan, W. R.; Celanović, I.; Soljačić, M.; Wang, E. N. A Nanophotonic Solar Thermophotovoltaic Device. *Nat. Nanotechnol.* **2014**, *9*, 126−130.
(23) Meléndez, J.; de Castro, A. J.; López, F.; Meneses, J. Spectrally Selective Gas Cell for Electrooptical Infrared Compact Multigas Sensor. *Sens. Actuators Phys.* **1995**, *47*, 417−421.
(24) Pralle, M. U.; Moelders, N.; McNeal, M. P.; Puscasu, I.; Greenwald, A. C.; Daly, J. T.; Johnson, E. A.; George, T.; Choi, D. S.; El-Kady, I.; et al. Photonic Crystal Enhanced Narrow-Band Infrared Emitters. *Appl. Phys. Lett.* **2002**, *81*, 4685.
(25) Laroche, M.; Carminati, R.; Greffet, J.-J. Coherent Thermal Antenna Using a Photonic Crystal Slab. *Phys. Rev. Lett.* **2006**, *96*, 123903.
(26) Inoue, T.; De Zoysa, M.; Asano, T.; Noda, S. Single-Peak Narrow-Bandwidth Mid-Infrared Thermal Emitters Based on Quantum Wells and Photonic Crystals. *Appl. Phys. Lett.* **2013**, *102*, 191110.
(27) Wan, J. T. K. Tunable Thermal Emission at Infrared Frequencies via Tungsten Gratings. *Opt. Commun.* **2009**, *282*, 1671−1675.
(28) Mason, J. A.; Adams, D. C.; Johnson, Z.; Smith, S.; Davis, A. W.; Wasserman, D. Selective Thermal Emission from Patterned Steel. *Opt. Express* **2010**, *18*, 25192−25198.
(29) Tsai, M.-W.; Chuang, T.-H.; Meng, C.-Y.; Chang, Y.-T.; Lee, S.-C. High Performance Midinfrared Narrow-Band Plasmonic Thermal Emitter. *Appl. Phys. Lett.* **2006**, *89*, 173116.
(30) Chan, G. H.; Zhao, J.; Schatz, G. C.; Duyne, R. P. V. Localized Surface Plasmon Resonance Spectroscopy of Triangular Aluminum Nanoparticles. *J. Phys. Chem. C* **2008**, *112*, 13958−13963.
(31) Ekinci, Y.; Solak, H. H.; Löffler, J. F. Plasmon Resonances of Aluminum Nanoparticles and Nanorods. *J. Appl. Phys.* **2008**, *104*, 083107.
(32) Zhou, L.; Gan, Q.; Bartoli, F. J.; Dierolf, V. Direct near-Field Optical Imaging of UV Bowtie Nanoantennas. *Opt. Express* **2009**, *17*, 20301−20306.
(33) Knight, M. W.; Liu, L.; Wang, Y.; Brown, L.; Mukherjee, S.; King, N. S.; Everitt, H. O.; Nordlander, P.; Halas, N. J. Aluminum Plasmonic Nanoantennas. *Nano Lett.* **2012**, *12*, 6000−6004.
(34) Knight, M. W.; King, N. S.; Liu, L.; Everitt, H. O.; Nordlander, P.; Halas, N. J. Aluminum for Plasmonics. *ACS Nano* **2014**, *8*, 834−840.
(35) Zhang, N.; Zhou, P.; Cheng, D.; Weng, X.; Xie, J.; Deng, L. Dual-Band Absorption of Mid-Infrared Metamaterial Absorber Based on Distinct Dielectric Spacing Layers. *Opt. Lett.* **2013**, *38*, 1125−1127.
(36) Sencer, A.; Ahmet Emin, T.; Andi, C.; Hasan, G.; Gokhan, B.; Aykutlu, D. Exploiting Native Al_2O_3 for Multispectral Aluminum Plasmonics. *ACS Photonics* **2014**, *1*, 1313−1321.
(37) Palik, E. D. *Handbook of Optical Constants of Solids*, 3rd ed.; Academic Press: New York, 1998.
(38) Rakic, A. D.; Djurišic, A. B.; Elazar, J. M.; Majewski, M. L. Optical Properties of Metallic Films for Vertical-Cavity Optoelectronic Devices. *Appl. Opt.* **1998**, *37*, 5271−5283.
(39) Kelf, T.; Sugawara, Y.; Cole, R.; Baumberg, J.; Abdelsalam, M.; Cintra, S.; Mahajan, S.; Russell, A.; Bartlett, P. Localized and Delocalized Plasmons in Metallic Nanovoids. *Phys. Rev. B* **2006**, *74*, 245415.

DOI: 10.1021/acsphotonics.5b00195
ACS Photonics 2015, 2, 964−970

(40) Hulteen, J. C.; Van Duyne, R. P. Nanosphere Lithography: A Materials General Fabrication Process for Periodic Particle Array Surfaces. *J. Vac. Sci. Technol. A* **1995**, *13*, 1553−1558.
(41) Chang, Y.-C.; Lu, S.-C.; Chung, H.-C.; Wang, S.-M.; Tsai, T.-D.; Guo, T.-F. High-Throughput Nanofabrication of Infra-Red and Chiral Metamaterials Using Nanospherical-Lens Lithography. *Sci. Rep.* **2013**, *3*, 3339.
(42) Walter, R.; Tittl, A.; Berrier, A.; Sterl, F.; Weiss, T.; Giessen, H. Large-Area Low-Cost Tunable Plasmonic Perfect Absorber in the Near Infrared by Colloidal Etching Lithography. *Adv. Opt. Mater.* **2015**, *3*, 398−403.

DOI: 10.1021/acsphotonics.5b00195
ACS Photonics 2015, 2, 964−970